# Generalized synchronization of chaos in directionally coupled chaotic systems

Nikolai F. Rulkov,* Mikhail M. Sushchik,† and Lev S. Tsimring‡
*Institute for Nonlinear Science, University of California, San Diego, Mail Code 0402, La Jolla, California 92093-0402*

Henry D. I. Abarbanel§
*Department of Physics and Marine Physical Laboratory, Scripps Institution of Oceanography, University of California, San Diego, Mail Code 0402, La Jolla, California 92093-0402*

(Received 15 August 1994)

Synchronization of chaotic systems is frequently taken to mean actual equality of the variables of the coupled systems as they evolve in time. We explore a generalization of this condition, which equates dynamical variables from one subsystem with a function of the variables of another subsystem. This means that synchronization implies a collapse of the overall evolution onto a subspace of the system attractor in full space. We explore this idea in systems where a response system $\mathbf{y}(t)$ is driven with the output of a driving system $\mathbf{x}(t)$, but there is no feedback to the driver. We lose generality but gain tractability with this restriction. To investigate the existence of the synchronization condition $\mathbf{y}(t)=\boldsymbol{\phi}(\mathbf{x}(t))$ we introduce the idea of mutual false nearest neighbors to determine when closeness in response space implies closeness in driving space. The synchronization condition also implies that the response dynamics is determined by the drive alone, and we provide tests for this as well. Examples are drawn from computer simulations on various known cases of synchronization and on data from nonlinear electrical circuits. Determining the presence of generalized synchronization will be quite important when one has only scalar observations from the drive and from the response systems since the use of time delay (or other) embedding methods will produce "imperfect" coordinates in which strict equality of the synchronized variables is unlikely to transpire.

PACS number(s): 05.45.+b, 84.30.Ng, 07.05.−t

## I. INTRODUCTION

Synchronization among dynamical variables in coupled nonlinear systems exhibiting chaotic motions would appear to be almost an oxymoron as the definition of chaos includes the rapid decorrelation of nearby orbits due to the instabilities throughout phase space. Nonetheless [1–3], it is quite straightforward to establish situations where synchronization occurs between signals, each of which is chaotic. This synchronization has clear applications to communications [4–6] and control [7,8]. Further, it may be responsible for the saturation of the invariant characteristics of chaos in chains of coupled nonlinear oscillators and in more complicated systems [9,10].

The synchronized chaotic oscillations, which have been most studied in the vast literature on the subject, are those where two coupled systems evolve according to exactly the same dynamics, that is, when the dynamical variables of the two systems are proportional to each other. There are two categories of systems where this sort of behavior is observed. The first category introduced by Pecora and Carroll [3,11] consists of a *driving* system, which exhibits chaotic behavior, and a *response* system. The latter is identical to the driving system except that some dynamical variables in it are set identically equal to the variables in the driving system. The second category includes coupled systems, which at zero coupling are identical to each other, and which each display chaotic behavior [1,2,12]. When the appropriate coupling is introduced, the systems exhibit identical oscillations associated with the onset of synchronization. Each of these categories represent degenerate cases, since the region in parameter space where this identity between driving and response systems can be observed is small indeed.

The development of a theoretical basis for synchronization of chaotic oscillations and for many of its practical applications calls for an expanded framework for synchronization. A step in this direction can be made by adopting the view of chaotic synchronization discussed by Afraimovich, Verichev, and Rabinovich [2]. Their viewpoint includes synchronization when the coupled chaotic systems are different and the form of coupling is unrestricted. Unfortunately, this general framework is difficult to convert into practical algorithms for analysis of chaotic synchronization in real physical systems.

In this paper, we limit ourselves to the less complicated case of forced synchronization between two coupled systems. The full system consists of an *autonomous driving* system and a *response* system. The chaotic dynamics of the driving system does not depend on the parameters of

*Electronic address: rulkov@hamilton.ucsd.edu
†Also at Department of Physics, University of California, San Diego, California.
Electronic address: mick@legendre.ucsd.edu
‡Electronic address: lev@legendre.ucsd.edu
§Also at Institute for Nonlinear Science, University of California, San Diego, California.
Electronic address: hdia@hamilton.ucsd.edu

 

the response system, so the connection between the systems is unidirectional. Let us call the vector of variables of the driving system $\mathbf{x}$ and the vector of variables of the response system $\mathbf{y}$. $\mathbf{x}$ is in the phase space of the driving system $\mathbf{D}$; $\mathbf{y}$, in the state space $\mathbf{R}$. If there is a transformation $\boldsymbol{\phi}$ from the trajectories of the attractor in $\mathbf{D}$ space to the trajectories in $\mathbf{R}$ space, we say the $\mathbf{x}$ and $\mathbf{y}$ systems are synchronized. The properties of this transformation do not depend upon the initial conditions in the basin of attraction of the system attractor. If we call the trajectory of the response system $\mathbf{y}(t)$, $\{\mathbf{y}\in\mathbf{R}\}$ and that of the driving system $\mathbf{x}(t)$, $\{\mathbf{x}\in\mathbf{D}\}$, then the transformation associated with synchronized motions on the overall chaotic attractor is $\mathbf{y}(t)=\boldsymbol{\phi}(\mathbf{x}(t))$. Clearly the orbits of the overall system lie in a subspace of the whole state space $\mathbf{D}\oplus\mathbf{R}$.

One typically studies only the case when $\boldsymbol{\phi}$ is the identity [1–3, 13–16]. In such a case, synchronization can be detected by looking at two variables, one chosen from the driving system and one from the response system. With a proper choice of these variables, call them $x_i(t)$ from the driving system and $y_i(t)$ from the response system, the synchronized motion becomes simply a sharp line in $y_i(t)$ versus $x_i(t)$ plane [3,13]. If the transformation $\boldsymbol{\phi}$ is richer, the projection may no longer be a line but may become a rather complicated geometrical object [17,18]. We call this kind of synchronized chaotic behavior *generalized synchronization,* and that is the matter we explore in this paper.

In this paper we describe a numerical method called *mutual false nearest neighbors,* which allows us to detect the presence of the continuous transformation $\boldsymbol{\phi}$ and thereby to distinguish between synchronized and unsynchronized behaviors of coupled chaotic systems. The method relies on the technique of time delay phase space reconstruction [19–21]. If a synchronizing relationship of the form $\mathbf{y}(t)=\boldsymbol{\phi}(\mathbf{x}(t))$ occurs, it means that the motion in the full $\mathbf{D}\oplus\mathbf{R}$ phase space has collapsed onto a subspace which is the manifold of synchronized motions. By observing the evolution of the response system in one scalar variable $r(t)$, we can reconstruct the chaotic trajectory $\mathbf{r}(t)$ in the embedding phase space $\mathbf{R}_E$ from $r(t)$ and its time delays using $d_r$ dimensional vectors

$$\mathbf{r}(t)=(r(t),r(t+T),r(t+2T),\ldots,r(t+(d_r-1)T)) , \tag{1}$$

and in that space, if synchronization occurs, we expect there to be a continuous functional relation

$$\mathbf{r}(t)=\boldsymbol{\psi}(\mathbf{d}(t)) , \tag{2}$$

where $\mathbf{d}(t)$ is the chaotic trajectory reconstructed in the embedding space $\mathbf{D}_E$ from scalar variables taken from the drive system. If $d_r$ is large enough, then, due to the existence of $\boldsymbol{\psi}$, many properties of the trajectories of the synchronized chaotic attractor in the embedding space $\mathbf{R}_E$ and of the related trajectories in $\mathbf{D}_E$ should be similar. In particular, any trajectories of the attractor generated in $\mathbf{D}_E$ which are close to each other will be unfolded into close trajectories in $\mathbf{R}_E$. So, to detect the existence of $\boldsymbol{\psi}$ we will explore the idea of mutual false nearest neighbors, which tests whether neighborliness in $\mathbf{D}_E$ translates in a practical, numerical sense to neighborliness in $\mathbf{R}_E$. To test this method, we apply it to a few examples where the transformation $\boldsymbol{\phi}$ is known. We also use the method to study generalized synchronization in an experiment with chaotic electronic circuits.

It is important to note that if there is a relationship $\mathbf{r}(t)=\boldsymbol{\psi}(\mathbf{d}(t))$ between the drive system orbits $\mathbf{d}(t)$ and the response system orbits $\mathbf{r}(t)$, then the critical characteristic of such synchronization is the ability to *predict* the response from observations of the drive [22]. Clearly, for practical applications of generalized synchronization, predictability is the crucial feature. In addition to the mutual false nearest neighbors test, we will examine aspects of the predictability of the coupled systems. Certainly when no relationship of the form suggested occurs, then observations of $\mathbf{d}(t)$ do not allow us to unambiguously determine the behavior of the response system $\mathbf{r}(t)$, and prediction of $\mathbf{r}(t)$ from $\mathbf{d}(t)$ will not work.

In Sec. II of this paper, we exhibit a class of systems that can be synchronized by a given driving signal when the transformation $\boldsymbol{\phi}$ is a known vector function or functional. The point of working with these "handmade" transformations is to emphasize that even when we have synchronized systems in which $\mathbf{y}(t)=\mathbf{x}(t)$ holds, observing the systems in another coordinate system may reveal a more structured and complex relationship among the variables. Since time delay embedding does not offer the luxury of choosing a set of coordinates in which synchronization need be so simple as $\mathbf{r}(t)=\mathbf{d}(t)$, it is important to recognize the effect of one's coordinate system on the decision about the existence of synchronization. In Sec. III, we describe the mutual false nearest neighbor algorithm which is one of our tests of the existence of the transformation $\boldsymbol{\phi}$. The result of its application to our test systems is also described. In Sec. IV, we apply the numerical method to characterize chaotic synchronization in an experiment with nonlinear electronic circuits. In Sec. V, we discuss other tests of the generalized synchronization based on the predictability of the response in a drive reconstructed phase space. Section VI contains our conclusions and additional discussion. An Appendix contains several general remarks about topics in the main body of the paper.

## II. EXAMPLES OF GENERALIZED SYNCHRONIZATION

We start with a description of a principle for synchronizing identical systems with individual chaotic behavior. The driving system is autonomous and satisfies

$$\frac{d\mathbf{x}(t)}{dt}=\mathbf{F}(\mathbf{x}(t)) . \tag{3}$$

In this paper we always consider coupling to the response system in the straightforward fashion

$$\frac{d\mathbf{y}(t)}{dt}=\mathbf{F}(\mathbf{y}(t))-\mathbf{G}\cdot(\mathbf{y}(t)-\mathbf{x}(t)) . \tag{4}$$

This form of the coupling always [13,23] allows simple

synchronized motion of the form

$$\mathbf{x}(t)=\mathbf{y}(t)\ , \tag{5}$$

which can be made stable by appropriate choices of the coupling matrix **G**.

The examples we look at in this section are artificial as we change the appearance of the synchronized motion by hand, but they provide a testbed for our numerical algorithms discussed below. Our requirement is to find methods to detect generalized synchronization and not just the identity relationship between driving and response variables, which ensues in the "correct" coordinates.

We begin with two systems synchronized by virtue of the coupling just shown, and then we apply a transformation into one of the coordinates, say **y**, to obtain new variables **z** in which the relationship expressing synchronization is more subtle. Since we know by construction that the systems are synchronized, our algorithms should be able to establish this fact even after the transformation. In this section we shall present a few examples illustrating this procedure. Some of these examples will be used later to test the numerical methods described in Secs. III and V. A more general formulation of this procedure can be found in the Appendix.

### A. Two examples of generalized synchronization

We now look at two examples that illustrate our main points more concretely. In the first, we consider two coupled Rössler oscillators: driving system,

$$\begin{aligned}\dot{x}_1&=(x_2+x_3)\ ,\\ \dot{x}_2&=x_1+0.2x_2\ ,\\ \dot{x}_3&=0.2+x_3(x_1-\mu)\ ,\end{aligned} \tag{6}$$

response system,

$$\begin{aligned}\dot{y}_1&=-(y_2+y_3)-g(y_1-x_1)\ ,\\ \dot{y}_2&=y_1+0.2y_2\ ,\\ \dot{y}_3&=0.2+y_3(y_1-\mu)\ ,\end{aligned} \tag{7}$$

with $\mu=5.7$.

The integral manifold

$$x_1=y_1\ ,\quad x_2=y_2\ ,\quad x_3=y_3\ , \tag{8}$$

which contains the trajectories of synchronized motions, is stable at $g=0.20$ and unstable at $g=0.15$. To confirm this we computed the conditional Lyapunov exponents [3,12] associated with nonautonomous behavior of the response system for these two values of the coupling parameter. The largest conditional Lyapunov exponent was $-0.021$ at $g=0.20$ and $+0.024$ at $g=0.15$.

Suppose we know only the variables $x_2$ and $y_2$ of these systems (6) and (7). Then a plot of $y_2$ versus $x_2$ will indicate the onset of synchronization when $y_2(t)=x_2(t)$. This plot for $g=0.20$, shown in Fig. 1(a), is a sharp straight line, as it should be for these synchronized oscillations (8). Figure 1(b) shows the same plot for $g=0.15$.

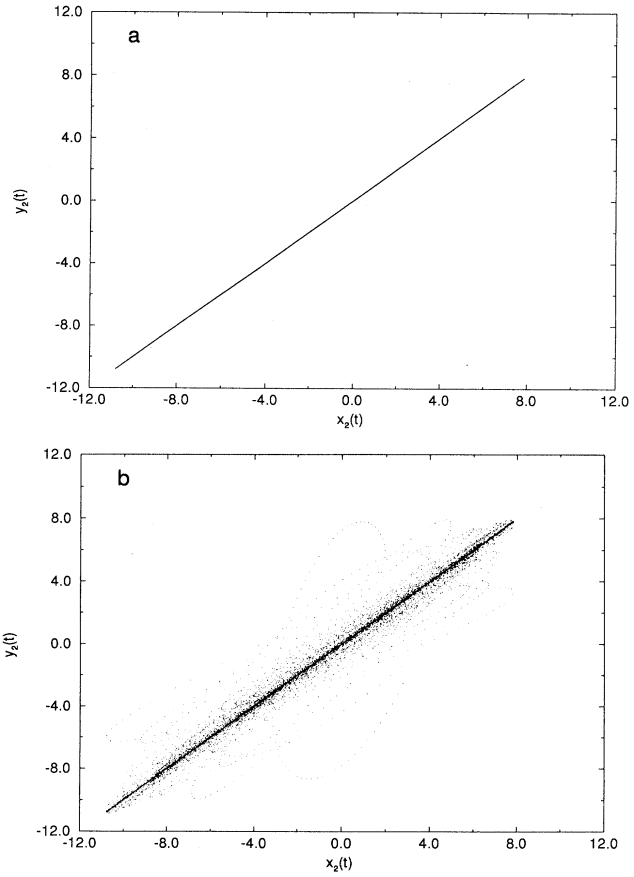


FIG. 1. The projection of the chaotic attractor generated by the system of Eqs. (6) and (7) onto the plane $(x_2,y_2)$: (a) synchronized behavior and (b) unsynchronized behavior.

Clearly this corresponds to unsynchronized motions in the coupled systems.

Now we construct a response system that exhibits *generalized synchronization* using the procedure described for a general case in the Appendix Sec. 1. We make the simple nonlinear transformation among the response variables

$$z_1=y_1\ ,\quad z_2=y_2+ay_3+by_3^2\ ,\quad z_3=y_3\ , \tag{9}$$

and we choose $a=0.4$ and $b=-0.008$ in what follows. This system should have the same characteristics as the original. The equations for this response system become

$$\begin{aligned}\dot{z}_1&=-[z_2+(1-a)z_3-bz_3^2]-g(z_1-x_1(t))\ ,\\ \dot{z}_2&=z_1+0.2(z_2-az_3-bz_3^2)\\ &\quad+(a+2bz_3)[0.2+z_3(z_1-\mu)]\ ,\\ \dot{z}_3&=0.2+z_3(z_1-\mu)\ .\end{aligned} \tag{10}$$

When we plot $z_2$ versus $x_2$ for the synchronized state at $g=0.20$, we no longer see a straight line but the more complex object in Fig. 2(a). The plot of $z_2$ versus $x_2$ for the synchronized state looks "cloudy" or "fuzzy."

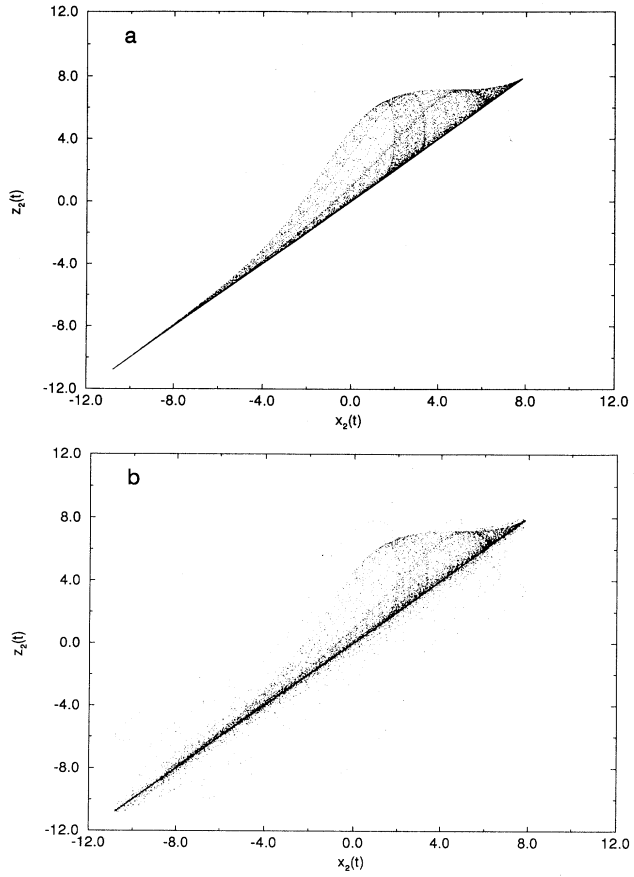


FIG. 2. The projection of the chaotic attractor generated by the system of Eqs. (6) and (10) on the plane $(x_2,z_2)$: (a) synchronized behavior and (b) unsynchronized behavior.

Nonetheless, since all we did was perform a smooth change of coordinates, we know that synchronization, as a basic property of these coupled oscillators, cannot have been lost. A similar plot for $g=0.15$, which corresponds to unsynchronized motions, is shown in Fig. 2(b).

In the second example, we consider chaotic synchronization in the two coupled nonlinear electronic circuits shown in Fig. 3. The chaotic dynamics of these circuits

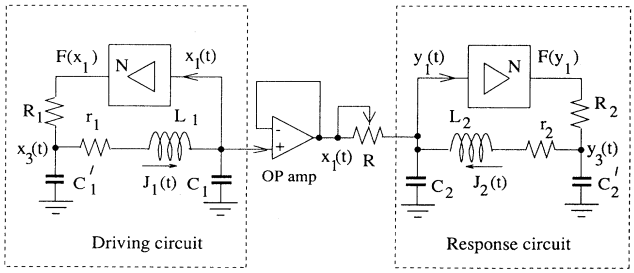


FIG. 3. The circuit diagram of the experiment with driving and response circuits. Nonlinear converters transform the input $X$ into the output $F(X)=\alpha_i f(X)$; see [12] for details. An operational amplifier is employed to provide unidirectional coupling. The value of the coupling is controlled by the resistor $R$.

has been studied in detail in [12,24]. Both driving and response circuits consist of a nonlinear converter and a linear feedback. The feedback includes the low pass filter $RC'$ and the resonant circuit $rLC$. The behavior of these two electronic circuits with *identical* parameters can be modeled by the following equations [13]: driving system,

$$\begin{aligned}\dot{x}_1&=x_2\ ,\\ \dot{x}_2&=-x_1-\delta x_2+x_3\ ,\\ \dot{x}_3&=\gamma[\alpha f(x_1)-x_3]-\sigma x_2\ ,\end{aligned}\tag{11}$$

response system,

$$\begin{aligned}\dot{y}_1&=y_2-g(y_1-x_1)\ ,\\ \dot{y}_2&=-y_1-\delta y_2+y_3\ ,\\ \dot{y}_3&=\gamma[\alpha f(y_1)-y_3]-\sigma y_2\ ,\end{aligned}\tag{12}$$

where $x_1(t)$, $x_3(t)$, $y_1(t)$, and $y_3(t)$ are the voltages across the capacitors $C_1$, $C_1'$, $C_2$, and $C_2'$, respectively. $x_2(t)=J_1(L_1/C_1)^{1/2}$ and $y_2(t)=J_2(L_2/C_2)^{1/2}$ with $J_i(t)$ the currents through the inductors $L_i$. $t=t_{\text{old}}(L_1C_1)^{-1/2}$. The nonlinear response of the converter, indicated by $f(x)$ in the equations, can be approximated by the piecewise nonlinear function

$$f(x)=\begin{cases}0.528, & \text{if } x\le -1.2\\ x(1-x^2), & \text{if } -1.2<x<1.2\\ -0.528, & \text{if } x\ge 1.2\ ,\end{cases}\tag{13}$$

and the parameter $\alpha$ entering the model equations is the gain of the nonlinear converter at $x_1=0$ $(y_1=0)$. The other parameters of the model are dependent on the linear feedback loop through

$$\gamma=\gamma_i=\frac{\sqrt{L_iC_i}}{R_iC_i'}\ ,\quad \delta=\delta_i=r_i\left[\frac{C_i}{L_i}\right]^{1/2}\ ,\quad \sigma=\sigma_i=\frac{C_i}{C_i'}\ ,\tag{14}$$

where index $i=1$ corresponds to the parameters of drive circuit and $i=2$ to the parameters of the response circuit, see Fig. 3. The strength of unidirectional coupling from one system to the other is controlled by $g=1/R(L_1/C_1)^{1/2}$. It is known [13] that the manifold of synchronized motions (8) is stable for $g$ higher than some critical value, which depends on the parameters of the circuit.

Again we make a transformation of coordinates on the response system. This time it is the linear change of variables

$$z_1=y_1\ ,\quad z_2=y_2\ ,\quad z_3=y_3-ay_2\ .\tag{15}$$

It is easy to verify that the response circuit equations produced by this transformation differs from the original one by the value of the parameters for the linear feedback and by having a different function for the nonlinear converter, namely,

$$\dot{z}_1 = z_2 - g(z_1 - x_1(t)) ,$$
$$\dot{z}_2 = -z_1 - \delta' z_2 + z_3 , \tag{16}$$
$$\dot{z}_3 = \gamma'[\alpha \tilde{f}(z_1) - z_3] - \sigma' z_2 ,$$

where

$$\delta' = \delta_1 - a,$$
$$\sigma' = \sigma_1 + a(\gamma_1 - \delta_1 + a) ,$$
$$\gamma' = \frac{\gamma_1}{1 + (a/\gamma_1)} , \tag{17}$$
$$\alpha \tilde{f}(z) = \frac{\alpha f(z) + (a/\gamma_1) z}{1 + (a/\gamma_1)} .$$

By construction, this new response circuit (16) is synchronized with the same driving system as above (11). Equations (11) and (16) describe two coupled nonlinear circuits both of which have the circuit diagrams shown in Fig. 3. The values of the parameters in the linear feedback of the response circuit and the characteristic of nonlinear converter are given by (17). In this case, even when the circuits are synchronized, the plot of the voltage across capacitor $C_2'$ versus the voltage across $C_1'$ has a rich structure as seen in Fig. 4, although the plot of voltages across capacitors $C_2$ and $C_1$ is still a straight line. The fact that two different chaotic circuits can be synchronized in a generalized sense is of significant practical importance because in practice we can never construct two absolutely identical circuits, and it is crucial for all applications to know that a parameter mismatch does not always destroy the manifold of synchronized motions, but may only change its shape.

### B. Systems obtained by an integral-algebraic transformation

The class of coordinate changes described above does not produce the most general family of response systems, which can be synchronized by a given driving system. We only allowed changes of coordinates local in time, so it excludes the possibility of synchronization with some time delay or some short-term memory. To illustrate how one can generalize the procedure described in the previous section to include these effects, we consider a preceding example.

To construct a system that will exhibit generalized synchronization with short-term memory, we employ the general strategy described in the Appendix Sec. 2. We start with the following driving and response systems for variables $\bar{\mathbf{x}}$ and $\bar{\mathbf{y}}$ correspondingly: driving system,

$$\dot{x}_1 = -(x_2 + x_3) ,$$
$$\dot{x}_2 = x_1 + 0.2 x_2 ,$$
$$\dot{x}_3 = 0.2 + x_3(x_1 - \mu) , \tag{18}$$
$$\dot{x}_m = -\gamma x_m + \alpha x_1 ,$$

response system,

$$\dot{y}_1 = -(y_2 + y_3) - g(y_1 - x_1) ,$$
$$\dot{y}_2 = y_1 + 0.2 y_2 ,$$
$$\dot{y}_3 = 0.2 + y_3(y_1 - \mu) , \tag{19}$$
$$\dot{y}_m = -\gamma y_m + \alpha y_1 ,$$

where $\gamma > 0$. System (18) and (19) are similar to the system of the two coupled Rössler Eqs. (6) and (7). The additional variables $x_m(t)$ and $y_m(t)$ introduce a short-term memory into the system. The equations that describe the dynamics of these variables decouple from the rest of the equations and one has for long times

$$x_m(t) = \alpha \int_{-\infty}^{t} e^{-\gamma(t-\tau)} x_1(\tau) d\tau ,$$
$$y_m(t) = \alpha \int_{-\infty}^{t} e^{-\gamma(t-\tau)} y_1(\tau) d\tau , \tag{20}$$

valid with exponential accuracy. Therefore, the introduction of $x_m$ and $y_m$ has no effect on synchronization in the system, and the driving system will synchronize the response system at the same values of $g$ as in the example with the two coupled Rössler systems. Now we follow the procedure from the preceding section to construct an equivalent response system, which is connected with the original one by the following transformation:

$$z_1 = y_1,$$
$$z_2 = y_2 + y_m = y_2 + \alpha \int_{-\infty}^{t} e^{-\gamma(t-\tau)} y_1(\tau) d\tau , \tag{21}$$
$$z_3 = y_3,$$
$$z_4 = y_m .$$

This construction leads to the new response system $\bar{\mathbf{z}}$;

$$\dot{z}_1 = -(z_2 + z_3 - z_4) - g(z_1 - x_1) ,$$
$$\dot{z}_2 = z_1 + 0.2(z_2 - z_4) - \gamma z_4 + \alpha z_1 ,$$
$$\dot{z}_3 = 0.2 + z_3(z_1 - \mu) , \tag{22}$$
$$\dot{z}_4 = -\gamma z_4 + \alpha z_1 .$$

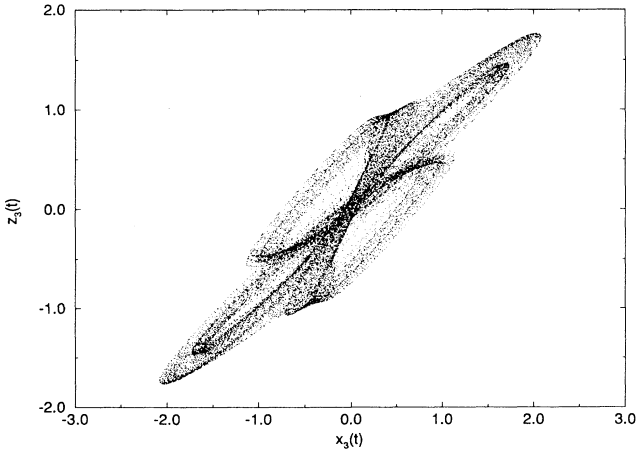


FIG. 4. The plot of voltage across capacitor $C_2'$ vs the voltage across capacitor $C_1'$; see Fig. 3. The data was obtained by numerical simulation of (11) and (12) with $\alpha = 32$, $\gamma = 0.1$, $\delta = 0.43$, $\sigma = 0.72$, $a = 0.4$, and $g = 1.0$.

Note that $x_m(t)$ still decouples from the rest of the equations and, therefore, can be omitted. Therefore, systems (6) and (22) are synchronized in a generalized sense when $g$ is such that systems (6) and (7) are synchronized. The system comprised of Eqs. (6) and (22) is an example of synchronization between two systems having a different number of degrees of freedom.

When the systems (18) and (19) are synchronized $\bar{\mathbf{x}}=\bar{\mathbf{y}}$, and it follows that the systems (6) and (22) are synchronized in the sense that

$$\begin{aligned} z_1 &= x_1 , \\ z_2 &= x_2 + \alpha \int_{-\infty}^{t} e^{-\gamma(t-\tau)} x_1(\tau) d\tau , \\ z_3 &= x_3 , \\ z_4 &= \alpha \int_{-\infty}^{t} e^{-\gamma(t-\tau)} x_1(\tau) d\tau . \end{aligned} \tag{23}$$

Figures 5(a) and 5(b) show the projections of the attractor in the combined *driving* + *response* space onto the $(x_2,z_2)$ plane. In all computations we used $\alpha=10$, and $\gamma=1$. Figure 5(a) presents the plot of $z_2$ versus $x_2$ for $g=0.20$. As in the case considered in Sec. II A, the plot looks very fuzzy. One can mistakenly draw the conclusion that the oscillations are not synchronized, while we just demonstrated the opposite. The plot of $z_2$ versus $x_2$ for $g=0.15$ corresponding to unsynchronized behavior is shown in Fig. 5(b).

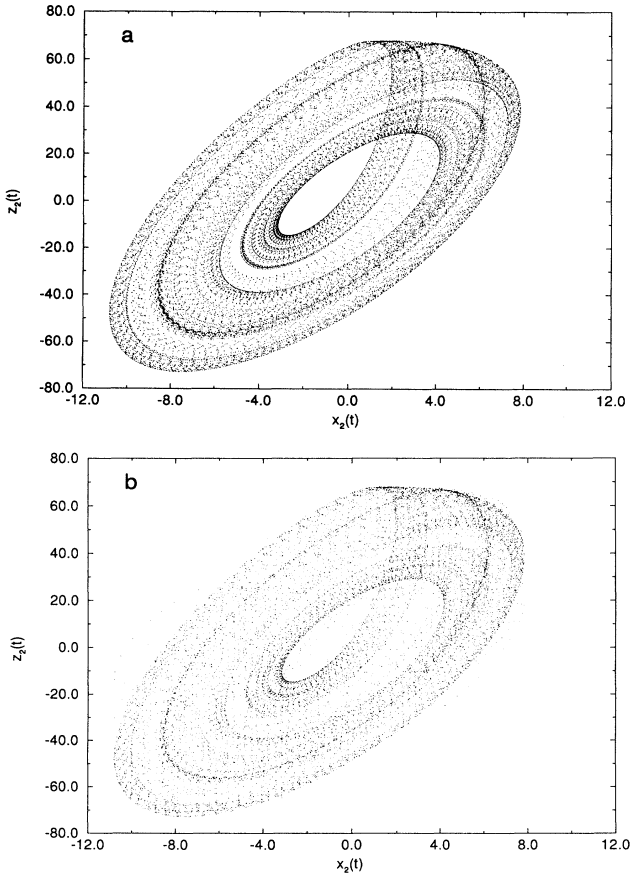


FIG. 5. The projection of the chaotic attractor generated by system (6) and (22) on the plane $(x_2,z_2)$: (a) synchronized behavior and (b) unsynchronized behavior.

Once again we have produced a "new" system from a known synchronized driving and response system by a change of variables which, of course, does not change the dynamics but only produces a different set of coordinates in which to view the dynamics. In the new coordinates, the appearance of synchronization is changed, and we need to test more than the equality of equivalent coordinates to uncover the synchronization between the systems. We now turn to some tests for this.

## III. MUTUAL FALSE NEAREST NEIGHBORS

By making changes of coordinates we demonstrated in the previous sections that simply looking for synchronization as the identity matching of drive and response variables $\mathbf{y}(t)=\mathbf{x}(t)$ will not uncover synchronization in general settings. For this we require an algorithm that rests on the existence of the generalized synchronization condition

$$\mathbf{y}(t)=\boldsymbol{\phi}(\mathbf{x}(t)) . \tag{24}$$

We have emphasized that it is this condition among drive variables $\mathbf{x}(t)$ and response variables $\mathbf{y}(t)$ that is the essence of synchronization of a driving and a response system. In this section we explore one requirement imposed by this connection; in the next section, we examine another. In our concluding section we will mention others that we have not yet explored.

The keystone of the characteristic of coupled systems that we are considering in this section is the concept of local neighborliness. When trajectories in the phase spaces of driving and response systems are connected by $\mathbf{y}(t)=\boldsymbol{\phi}(\mathbf{x}(t))$, two *close* states in the phase space of the response system correspond to two *close* states in the space of the driving system. Let us consider a set of points in the spaces of the coupled systems coming from finite segments of trajectories sampled at moments of time $t_n=nt_{\text{sampling}}$ where $n$ is integer. For simplicity, we shall look at the case when the transformation $\boldsymbol{\phi}$ is algebraic. Pick an arbitrary point $\mathbf{x}_n=\mathbf{x}(t_n)$ in the phase space of the driving system. Suppose the nearest phase space neighbor of this point has time index $n_{\text{NND}}$. Then as long as the trajectories are connected by relation (24) the point $\mathbf{y}_n$ in the space of the response system will have point $\mathbf{y}_{n_{\text{NND}}}$ a close neighbor.

In a few words, what we are looking for is a geometric connection between the driving and response systems which preserves the identity of neighborhoods in state space. This is a kind of correlation between observed dynamical variables, one from the driving system and one from the response system. It is not a linear correlation, of course, as the underlying dynamics is nonlinear. We could cast the statistical tests we are about to consider in terms of correlations between response and driving variables. If we were to do so, we would probably prefer to seek a nonlinear correlation among these variables using

a statistic similar to mutual information [21]. This is quite computationally intensive, and for our purposes we have found the statistics below to be adequate, if not fully nonlinear. Indeed, they emphasize the geometry more than the nonlinearity of the dynamics.

This property can be characterized by a numerical parameter. To form this parameter we notice that when relation (24) holds and the distances between two nearest neighbors in the phase spaces of the driving and response systems are small, we can write

$$\mathbf{y}_n-\mathbf{y}_{n_{\mathrm{NND}}}=\boldsymbol{\phi}(\mathbf{x}_n)-\boldsymbol{\phi}(\mathbf{x}_{n_{\mathrm{NND}}})\approx\mathbf{D}\boldsymbol{\phi}(\mathbf{x}_n)(\mathbf{x}_n-\mathbf{x}_{n_{\mathrm{NND}}}) , \tag{25}$$

where $\mathbf{D}\boldsymbol{\phi}(\mathbf{x}_n)$ is the Jacobian matrix of transformation $\boldsymbol{\phi}$ evaluated at location $\mathbf{x}_n$. Similarly we go to time index $n$ and observe the response vector $\mathbf{y}_n$ and locate its nearest neighbor $\mathbf{y}_{n_{\mathrm{NNR}}}$ which comes at time index $n_{\mathrm{NNR}}$. Again, when $\mathbf{y}(t)=\boldsymbol{\phi}(\mathbf{x}(t))$ we can write

$$\mathbf{y}_n-\mathbf{y}_{n_{\mathrm{NNR}}}=\boldsymbol{\phi}(\mathbf{x}_n)-\boldsymbol{\phi}(\mathbf{x}_{n_{\mathrm{NNR}}})\approx\mathbf{D}\boldsymbol{\phi}(\mathbf{x}_n)(\mathbf{x}_n-\mathbf{x}_{n_{\mathrm{NNR}}}) . \tag{26}$$

This suggests that the ratio

$$\frac{|\mathbf{y}_n-\mathbf{y}_{n_{\mathrm{NND}}}|}{|\mathbf{x}_n-\mathbf{x}_{n_{\mathrm{NND}}}|}\frac{|\mathbf{x}_n-\mathbf{x}_{n_{\mathrm{NNR}}}|}{|\mathbf{y}_n-\mathbf{y}_{n_{\mathrm{NNR}}}|} , \tag{27}$$

which we call the *mutual false nearest neighbors* (MFNN) parameter, should be of the order of unity when the systems are synchronized in the sense that $\mathbf{y}(t)=\boldsymbol{\phi}(\mathbf{x}(t))$. Generally, if the synchronization relation $\mathbf{y}(t)=\boldsymbol{\phi}(\mathbf{x}(t))$ does not hold, then this parameter should on average be of order (size of attractor squared)/(distance between nearest neighbors squared).

In experiments, we usually do not have the luxury of working with the actual vectors of phase space variables. Normally only the time series of a single variable is available to characterize the behavior of each system. Therefore, to be able to analyze experimental as well as numerical data we will rely upon the phase space reconstruction method [21].

Suppose we have observed a scalar time series $r(n)$ of some variable in the response system. We form the response vector

$$\mathbf{r}(n)=(r(n),r(n-T_r),r(n-2T_r),\ldots,r(n-(d_r-1)T_r)) , \tag{28}$$

where $T_r$ is an integer multiple of the sampling time for the observations of the response system. $T_r$ is selected by average mutual information [21]. We call the $d_r$ dimensional space associated with these vectors $\mathbf{R}_E$. We also observe a scalar time series $d(t)$ of a variable from the driving system and form the vector

$$\mathbf{d}(m)=(d(m),d(m-T_d),\times d(m-2T_d),\ldots,d(m-(d_d-1)T_d) , \tag{29}$$

where $T_d$ is an integer multiple of the sampling time for the observations of the driving system. We call the space of these vectors $\mathbf{D}_E$. $d_r$ and $d_d$ are each larger than the respective global embedding dimensions required to unfold the response and the driving attractors, respectively.

By Takens' theorem, the attractor in embedding space $\mathbf{D}_E$ inherits all properties of the attractor of the driving system. Similarly, when the coupling is not zero, the attractor in the embedding space $\mathbf{R}_E$ is equivalent to the attractor of the whole system; *driving + response.* When there is a transformation $\boldsymbol{\phi}$ that relates the trajectories in the subspaces of the driving and response systems, there must also be a transformation that relates the trajectory in the phase space of the driving system to that in the phase space of the combined system *driving + response.* Therefore, the conclusions made above concerning the properties of nearest neighbors for synchronized and unsynchronized behaviors are still true when they are applied to the reconstructed spaces $\mathbf{D}_E$ and $\mathbf{R}_E$.

At the same time, using the language of embedding space reconstruction, we can give now a different interpretation to this property. A criterion similar to the one we use here forms the basis of the false neighbors method for determining the minimum dimension that is required to unfold the attractor without self-crossing of the trajectories when one uses embedding methods to reconstruct the attractor from time series [25]. In the false neighbors method, one embeds the time series in a $k$-dimensional space and finds pairs of nearest neighbors. Then the time series is embedded in a space of dimension $k+1$ and the points, which were nearest neighbors in $k$ space, are traced into the new space. When the attractor is fully unfolded in $k$ space, the two spaces present equivalent characterizations of the attractor. However, if the attractor is not unfolded in $k$ space and is unfolded in $(k+1)$ space some pairs of points, called false neighbors, that were nearest neighbors in $k$ space will no longer be nearest neighbors in $(k+1)$ space. A similar picture is observed when we consider points in the embedding space of the driving signal and points in the embedding space of the response signal. If $\mathbf{r}(t)$ can be obtained by a transformation of $\mathbf{d}(t)$, that is, the response system is synchronized, then the attractors constructed in spaces $\mathbf{R}_E$ and $\mathbf{D}_E$ can be considered as different embeddings of the same attractor, and because of Takens' theorem each provides an equally appropriate set of coordinates. Therefore, if points with time indices $n$ and $n_{\mathrm{NND}}$ were nearest neighbors in $\mathbf{D}_E$ space, they will be close neighbors in $\mathbf{R}_E$ space too.

Thus, we argued that the points in the embedding spaces possess the same neighborliness properties as points in the original spaces of physical variables, and we can conclude that the MFNN parameter can be computed according to (27) even when it is computed using the trajectories in embedding spaces of driving and response instead of trajectories in original spaces of $\mathbf{x}$ and $\mathbf{y}$. When the systems are synchronized and $d_r$ and $d_d$ are large enough, the MFNN parameter should be of order one at all locations. When the systems are not synchronized, this parameter is expected to be large at some locations on the attractor.

On further consideration, we find that this test has a

few problems which are connected with the nontrivial scaling of the MFNN parameter with the embedding dimensions of driving and response. There are two causes for these problems, both of which can make the practical value of this test questionable. First of all, when we use a time series of fixed length the average distance between the nearest neighbors becomes larger and is comparable with the size of the attractor in high embedding dimensions. As a result, the denominator of (27) grows with increasing embedding dimension. The numerator for *unsynchronized* trajectories is always of the order of the square of the size of the attractor and, therefore, the ratio itself may become small as the embedding dimension increases, even if there is no synchronized motion in the system. On the other hand, when a time series of fixed length is embedded in spaces of higher and higher embedding dimensions, the population density in the spaces decreases. Eventually this leads to loss of any fine structure at high embedding dimensions. The nearest neighbor that is found in high-dimensional space may no longer be a close neighbor. As a result, it becomes more and more difficult to uncover a connection between two trajectories when there is such a connection. The MFNN parameter defined by (27) can be large even when the systems are synchronized.

Thus, the variation of the parameter with embedding dimensions occurs for two reasons. (1) The search for neighbors is performed in spaces of changing dimensions, and (2) the distances are computed in the spaces of changing dimensions. The former cannot be helped. However, without changing the main idea, we can change the test so that all distances are computed in the same space.

The modified MFNN parameter, which we will use throughout the rest of the paper, is constructed as follows. We embed the response time series in the space $\mathbf{R}_E$ of dimension $d_r$, which is then fixed. $d_r$ must not be less than the minimum dimension necessary to unfold the attractor corresponding to the response time series. All distances will be computed in this space. $d_d$ is variable and is larger than the minimum dimension needed to unfold the driver attractor without self-crossing. For each $d_d$, we go to time index $n$ and locate the nearest neighbor of point $\mathbf{d}(n)$, which comes at time index $n_{\mathrm{NND}}$. We also find the nearest neighbor $\mathbf{r}(n_{\mathrm{NNR}})$ of point $\mathbf{r}(n)$ in the response embedding space. Then, we form the ratio

$$\frac{|\mathbf{r}(n)-\mathbf{r}(n_{\mathrm{NND}})|^2}{|\mathbf{r}(n)-\mathbf{r}(n_{\mathrm{NNR}})|^2}\ , \tag{30}$$

which is a less symmetric form of (27). We evaluate the squares of Cartesian distances instead of the distances themselves to reduce the computation time. Finally, to compensate for the increase of the MFNN parameter in high dimensions due to the sparseness of the phase space population, we divide (30) by the same parameter, computed for the driving time series. This brings us to the final form of the MFNN parameter

$$P(n,d_r,d_d)=\frac{|\mathbf{d}'(n)-\mathbf{d}'(n_{\mathrm{NND}}')|^2}{|\mathbf{d}'(n)-\mathbf{d}'(n_{\mathrm{NND}})|^2}\frac{|\mathbf{r}(n)-\mathbf{r}(n_{\mathrm{NND}})|^2}{|\mathbf{r}(n)-\mathbf{r}(n_{\mathrm{NNR}})|^2}\ , \tag{31}$$

where $\mathbf{d}'$ are vectors of the driving time series embedded in the space of dimension $d_r$ and $\mathbf{d}'(n_{\mathrm{NND}'})$ is the nearest neighbor of point $\mathbf{d}'(n)$ in this $d_r$ dimensional space. This parameter should on the average be of order unity for synchronized trajectories. $P(n,d_r,d_d)\gg 1$ for unsynchronized trajectories. From now on we will refer to this quantity as the mutual false nearest neighbor parameter.

It should be understood that $P(n,d_r,d_d)$ is a local characteristic of the attractor in the combined $\mathbf{D}_E\oplus\mathbf{R}_E$ space. To obtain reliable information about the regime in which the system evolves as synchronized or unsynchronized motion, we must determine a statistical ensemble of MFNN values computed at a number of locations on the attractor. Examining the statistical distribution of MFNN is especially important when one studies the system close to the onset of synchronization. In many cases, synchronized chaotic motions appear after an intermittent regime in which the system evolves nearly on the manifold of synchronized motions, but leaves it for short periods of time during unsynchronized outbursts. In this case, $P(n,d_r,d_d)$ will be of order unity at almost all points but will become large at a small number of points corresponding to these outbursts. Thus, it is very instructive to study the histograms of a set of MFNN parameters to obtain the maximum information about the system.

However, as we shall demonstrate in the following sections, one can distinguish between synchronized and unsynchronized behaviors by studying the average value $\bar{P}(d_r,d_d)$ of the MFNN parameter alone.

### Testing mutual false nearest neighbors

To check the effectiveness of the mutual false nearest neighbor method, we apply it to the systems (6) and (10), and (6) and (22). In each of the calculations discussed in this section, we used a total of 60 000 data points. We employed a fourth-order Runge-Kutta integrator with time step 0.02 to generate the data, and the data was sampled with time step 0.8. The time delays $T_r$ and $T_d$ were each taken to be five. The embedding dimension $d_r=4$ was selected, according to the method described in [21,25], and only $d_d$ was varied in our calculations. We computed $P(n,d_r,d_d)$ at 10 000 different locations on the attractor and used them to evaluate the average values $\bar{P}(d_r,d_d)$ of the MFNN parameter. Figures 2 and 5 display the dependence of drive versus response time series for systems and (6) and (10), and (6) and (22), respectively, for the case when the synchronization manifold is stable and for the case when it is not. In the latter situation, the synchronization is disrupted with outbursts away from the synchronization manifold. These outbursts, which have an intermittent character, are frequently observed close to the onset of synchronization of chaotic motions [26,27]. For comparison we refer to similar plots for two identical coupled Rössler attractors (6) and (7), as shown in Fig. 1. One can see that plots in Figs. 2(a) and 5(a) look very fuzzy, making it hard to identify synchronization by traditional subjective methods.

Figure 6 shows $\bar{P}(d_r=4,d_d)\equiv\bar{P}(d_d)$ as a function of

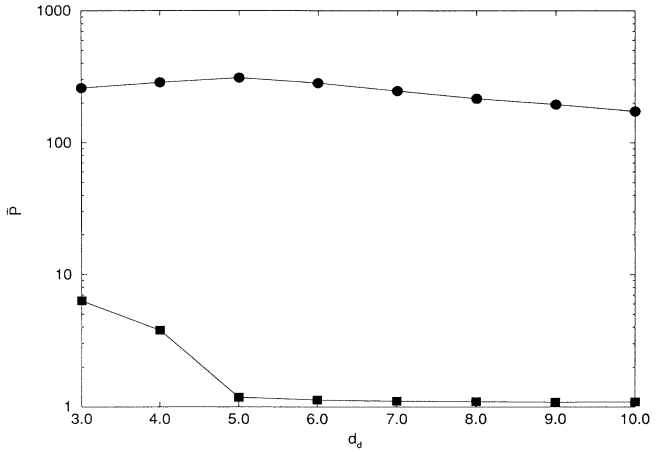


FIG. 6. $\bar{P}(d_d)$ as a function of $d_d$ for different values of the coupling parameter for the time series generated by the system of Eqs. (6) and (10): squares, synchronized behavior at $g=0.2$; circles, unsynchronized behavior at $g=0.15$.

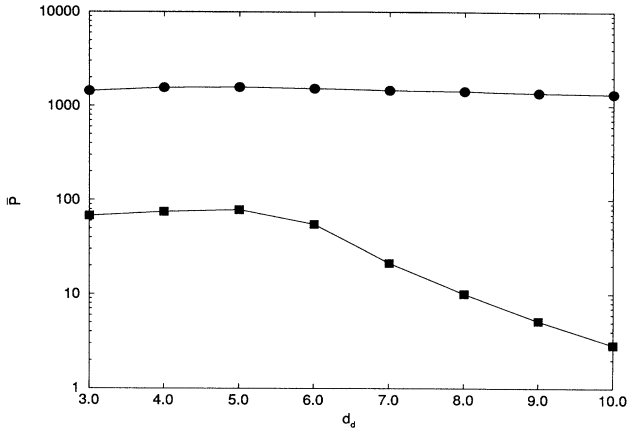


FIG. 8. $\bar{P}(d_d)$ as a function of $d_d$ for different values of the coupling parameter for the time series generated by the system of Eqs. (6) and (22): squares, synchronized behavior at $g=0.2$; circles, unsynchronized behavior at $g=0.15$.

$d_d$ for the system of Eqs. (6) and (10) with $a=0.4$ and $b=-0.008$. In this case, the transformation that maps the drive phase space onto the full phase space is purely algebraic and, therefore, when the systems are synchronized, $\bar{P}(d_d)$ drops to unity as soon as the $d_d$ embedding dimension is high enough to unfold both drive and response time series. When the synchronization manifold loses its stability, $\bar{P}(d_d)$ stays large at all $d_d$. Figure 7 shows $[\bar{P}(d_d=10)]^{-1}$ as a function of the coupling coefficient $g$ in (10). From the plot alone, one can conclude that chaotic motions in the system are synchronized for $g \geq 0.2$ and unsynchronized for $g \leq 0.16$ and that the actual transition to synchronized chaotic behavior occurs somewhere in the interval $0.16 < g < 0.2$. The curve is smeared in this interval as a result of the intermittency discussed above.

For the system of (6) and (22) with $\alpha=10$ and $\gamma=1$, the behavior of $\bar{P}(d_d)$ is more complicated. As shown in Fig. 8, for synchronized time series, $\bar{P}(d_d)$ computed with $d_r=6$ does not reach unity at any finite dimension but seems to approach it in the limit of $d_d \to \infty$. This behavior is expected, since the presence of the fourth equation in (22) implies that the transformation from the drive phase space to the phase space of the full system has a cumulative character. Note, that although we could use a local transformation in the phase space of $\tilde{\mathbf{y}}$ to obtain the modified response system (22), the transformation from $\mathbf{x}$ to $\tilde{\mathbf{z}}$ does have a cumulative integral character. This is because there is no feedback from the $x_m$ equation to the rest of system (18). Therefore, we cannot reconstruct the full $\tilde{\mathbf{x}}$ space using the time series of any of the $\mathbf{x}$ components alone. Nevertheless, one can see that as $d_d$ increases, $\bar{P}(d_d)$ decreases monotonically to unity, and this behavior signals the presence of chaotic synchronization. For a different coupling parameter, when the synchronization is lost, $\bar{P}(d_d)$ is large and stays large.

Thus, mutual false nearest neighbors prove to be quite a promising tool for the characterization of chaotic synchronization. In the next section we will demonstrate how this method works when applied to synchronization in a laboratory electronic circuit.

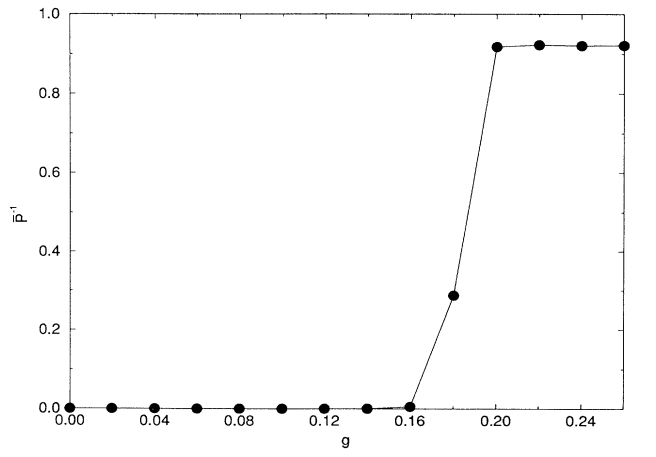


FIG. 7. $\bar{P}^{-1}$ computed at $d_d=10$ as a function of the coupling parameter $g$ in (10).

## IV. GENERALIZED SYNCHRONIZATION OF TWO CHAOTIC CIRCUITS

Next we present the results of our study of chaotic synchronization in experiments with electronic circuits. The circuit diagram of driving and response circuits coupled by the resistor $R$ is shown in Fig. 3. We discussed these circuits briefly in Sec. II. The insertion of an operational amplifier into the coupling between the circuits assures that the coupling is one way; namely, from the driving circuit to the response circuit. In our experiment the parameters of the circuits were chosen to be $C_1=334$ nF, $C_2=331$ nF, $C_1'=221$ nF, $C_2'=219$ nF, $L_1=L_2=144.9$ mH, $R_1=4.01$ kΩ, and $\alpha_1=\alpha_2=22.5$. The values of $R_2$ and $R$ serve as control parameters. Data from driving

and response circuits were collected with a sampling rate 50 $\mu$s.

The chaotic attractor generated by the drive circuit is shown in Fig. 9 as a projection onto the $(x_1,x_3)$ plane. When the parameters of the response circuit are tuned to be the same as those of the driving circuit ($R_2=R_1$), and the coupling is strong enough, the circuits produce identical synchronized chaotic oscillations. This synchronized behavior can be easily detected by the analysis of projection of the trajectory onto the plane of the variables $(x_1,y_1)$, as one can see in Fig. 10(a). This plot shows a straight line, which is a projection of the manifold of synchronized motions. When the coupling becomes less than some critical value ($R \simeq 0.35$ k$\Omega$) the manifold loses stability and the chaotic oscillations in the response circuit become unsynchronized. The projection onto the $(x_1,y_1)$ plane for $R=1.0$ k$\Omega$ is shown in Fig. 10(b) for the unsynchronized oscillations.

It was shown in Sec. II and in [28] that the circuits can display generalized synchronization. To investigate the transition from this generalized synchronization to unsynchronized oscillations, we detune the parameter $R_2$ in the response circuit to the value $R_2=2.71$ k$\Omega$ and study chaotic motions generated by the circuits for different values of coupling parameters. The chaotic attractors corresponding to synchronized and unsynchronized oscillations, which occur for two different values of coupling parameter, are shown in Fig. 11.

In order to test for the existence of the functional relation between driving and response trajectories, which indicates synchronized chaotic behavior of the circuits with different parameters, we employ the MFNN analysis just described. We used 17 000 data points in each time series for phase space reconstruction, which was done with $T_r=T_d=5$ and $d_r=5$. Various $\bar{P}(d_d)$ calculated from the data generated by the circuits for different values of the coupling parameter are presented in Fig. 12. When $R$ equals zero and 0.15 k$\Omega$, $\bar{P}(d_d)$ remains close to unity for large $d_d$, and clearly indicates synchronization between the driving and the response circuits. For data with $R$ equal to 1.0 and 0.5 k$\Omega$, large values of $\bar{P}(d_d)$ at high $d_d$ means that the motions in the circuits are unsynchronized.

Figure 13 depicts $(\bar{P})^{-1}$ for $d_d=10$ as a function of the resistance $R$ of the coupling. One can see that this parameter is small for $R=0.5-1.0$ k$\Omega$, which corresponds to completely unsynchronized motion, and saturates at about 0.6–0.7 when the coupling is strong $0.0 \leq R \leq 0.2$ k$\Omega$ indicating the onset of synchronization. The transition interval 0.2 k$\Omega < R < 0.5$ k$\Omega$ corresponds to intermittent behavior.

## V. PREDICTABILITY TESTS FOR GENERALIZED SYNCHRONIZATION

The fact that a functional relationship between the signals from the driving system and the signals from the response system exists suggests that this function $\phi$ can be found and used for prediction purposes. Indeed, if two

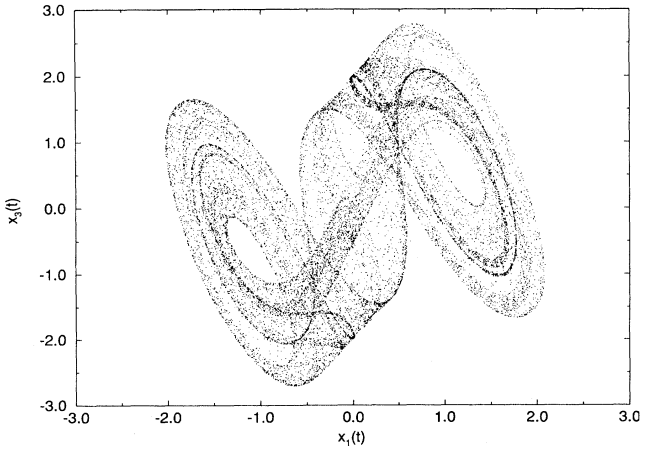


FIG. 9. The projection of the chaotic attractor onto the plane $(x_1,x_3)$. These are measurements from the driving circuit.

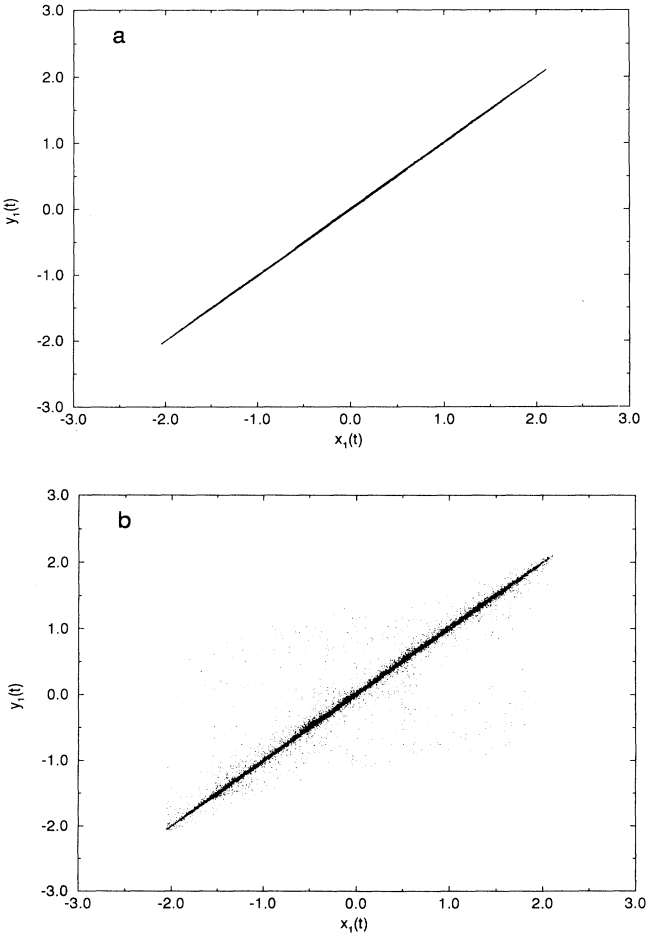


FIG. 10. The projection of the chaotic attractor on the plane $(x_1,y_1)$ measured from the circuits with identical parameters: (a) synchronized motions ($R=0.2$ k$\Omega$) and (b) unsynchronized motions ($R=1.0$ k $\Omega$).

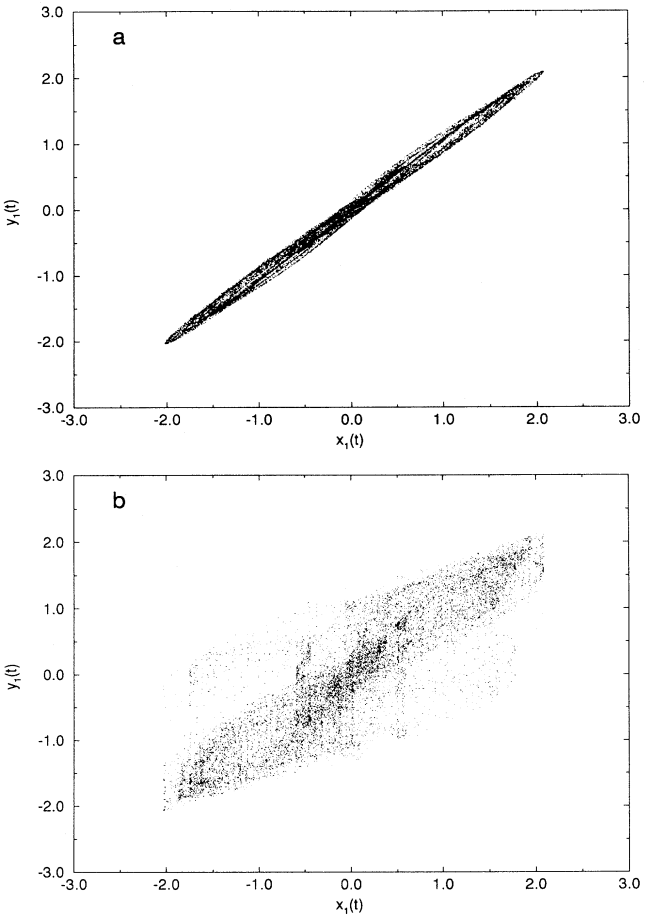


FIG. 11. The projection of the chaotic attractor on the plane $(x_1,y_1)$ measured from the circuits with different parameters; (a) synchronized motions ($R=0.15$ kΩ) and (b) unsynchronized motions ($R=0.5$ kΩ).

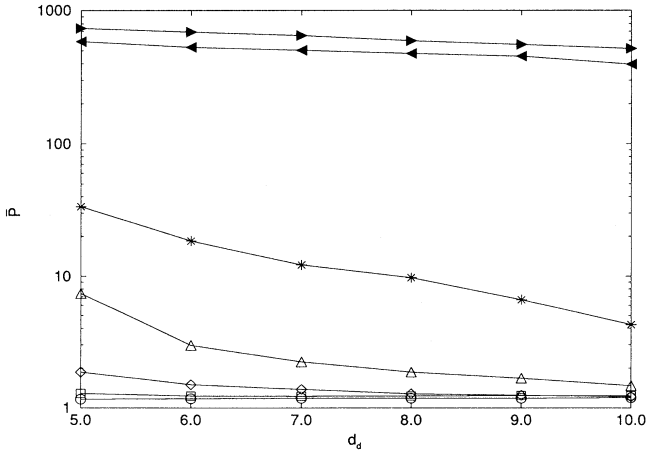


FIG. 12. $\bar{P}(d_d)$ as a function of $d_d$ for the data collected from the coupled electronic circuits: circles, $R=0.00$ kΩ; squares, $R=0.10$ kΩ; diamonds, $R=0.15$ kΩ; triangles up, $R=0.20$ kΩ; stars, $R=0.3$ kΩ; triangles left, $R=0.50$ kΩ; triangles right, $R=1.00$ kΩ.

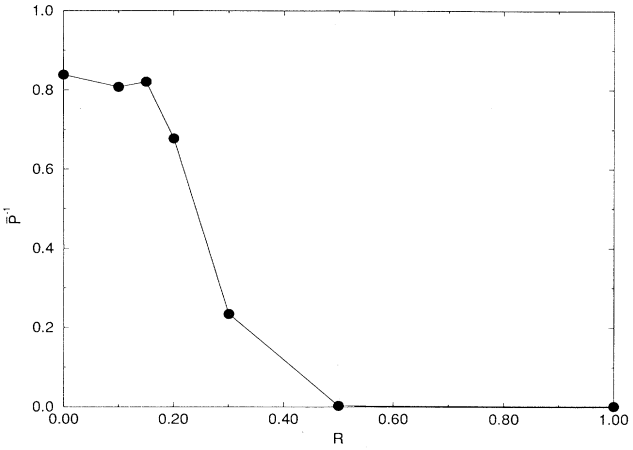


FIG. 13. $\bar{P}^{-1}$ computed at $d_d=10$ as a function of the coupling resistor $R$ for the experiment with coupled electronic circuits.

systems are synchronized, then the state of the response system can be predicted solely by knowing the state of a driver, even if the relation between two variables is rather complicated and unknown. A similar idea was explored in [22] where it was demonstrated that two different variables from *one* low-dimensional chaotic system can be predicted in terms of one another by reconstructing their functional relation in an appropriate embedding space. For the reconstruction, one needs a segment of simultaneous measurements of both variables.

The same approach can be used here. We will be looking for a connection

$$r(n)=G(\mathbf{d}(n)) , \tag{32}$$

which we can deduce working in the embedding space of the driving system. We assume its dimension to be high enough to unfold the attractor of the driver. Here $\mathbf{d}(n)$ is a vector formed from a scalar time series $d(n)$ in accordance with

$$\mathbf{d}(m)=(d(m),d(m-T_d), \times d(m-2T_d),\ldots,d(m-(d_d-1)T_d)) . \tag{33}$$

To find this connection we must have some simultaneous measurements of $d(n)$ and $r(n)$. If such a reconstruction is indeed possible, it signals that the driver and the response are synchronized. If the errors in the prediction become large, that means that there is no synchronization. There are a number of algorithms developed for functional reconstruction [21]. We used here the same algorithm as in [22]—local polynomial mappings. In fact, we needed only local linear maps in our work. In this approach, the nonlinear function $G(\mathbf{x})$ is represented as a collection of local polynomial maps, different for different neighborhoods in the phase space. The parameters of each map are determined by a least squares fit using known simultaneous measurements of $d(n)$ and $r(n)$. It involves searching through these time series and finding those vectors that are neighbors of a given vector $\mathbf{d}(n)$ in the embedding space.

In order to test the predictive ability of our model, we divide our data into two segments. The first segment of $N_T$ pairs $\{d(n),r(n)\}$ we use for model "training." At the remaining $N_R = N - N_T$ pairs, we compare the predicted values $r_p(n)$ with the measured values $r(n)$ point by point. The difference

$$\eta(n) = (r(n) - r_p(n))/\Delta(r) \tag{34}$$

is a useful measure of the quality of prediction. We normalize here by the standard deviation $\Delta(r)$ of the response signal. In the present case, for a properly chosen time delay and high enough embedding dimension, it characterizes primarily the presence of synchronization. In Fig. 14, we show this difference for the experimental data from the electronic circuit for two values of the coupling parameter. One can see that at $R = 0.20$ kΩ the magnitude of the variations is significantly reduced as compared to the case $R = 0.30$ kΩ. Intermittent bursts of fluctuations are also clearly seen here. An analogous intermittent picture is observed for numerically generated data from the coupled Rössler systems. For $R \leq 0.15$ kΩ, the prediction error $\eta(n)$ decreases sharply and does not exceed 0.2.

It is convenient to characterize the average quality of prediction by

$$Q = \frac{\langle (r(n) - r_p(n))^2 \rangle}{2\langle (r(n) - \langle r(n) \rangle)^2 \rangle} = \frac{\langle \eta(n)^2 \rangle}{2}, \tag{35}$$

where

$$\langle \cdots \rangle = \frac{1}{N_R} \sum_{i=1}^{N_R} . \tag{36}$$

$Q$ should be very small for complete synchronization and will be $O(1)$ if the quality of prediction is very poor; that is, $r(n)$ and $r_p(n)$ are not correlated. In Figs. 15(a) and 15(b) we present this parameter $Q$ as a function of the coupling parameter for coupled Rössler systems [Fig. 15(a)] and resistance for coupled electronic circuits [Fig. 15(b)]. In agreement with the MFNN test, we observe a sharp transition from the synchronized state to unsyn-

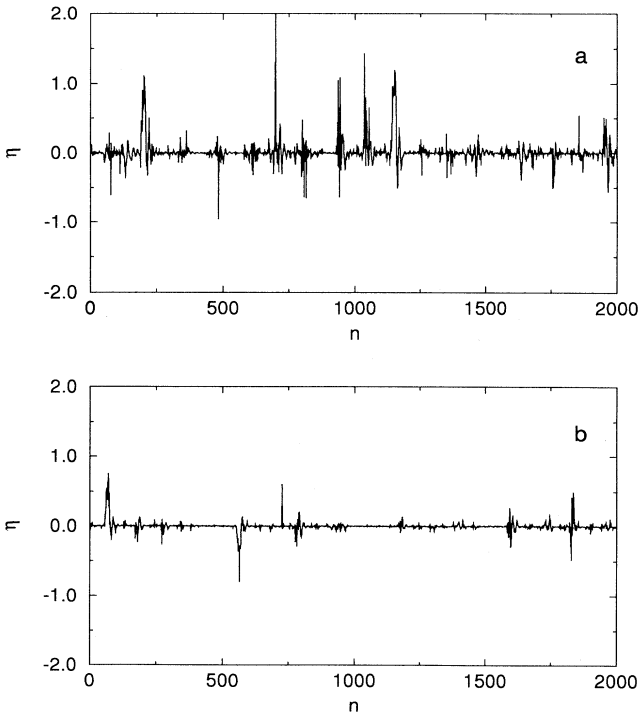


FIG. 14. Prediction error $\eta(n)$ as a function of $n$ for the experimental data from two coupled electronic circuits. Local linear predictor in the four-dimensional embedding space were built using a learning set of 10 000 pairs $\{d(n),r(n)\}$, time delay $T = 5$: (a) $R = 0.3$ and (b) $R = 0.2$. Sporadic bursts of large errors associated with regions of desynchronization on the attractor, are seen in both cases; however in (b) case they are weaker and sparser.

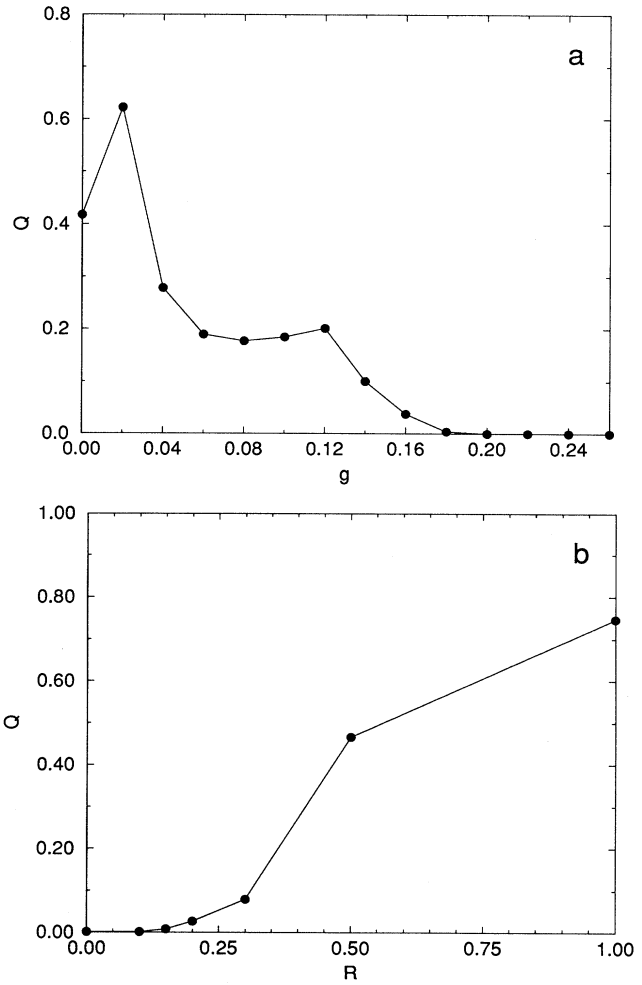


FIG. 15. Averaged relative prediction error $Q$ computed by formula (35) for the coupled Rössler systems (a) and coupled electronic circuits (b) vs control parameter: $g$ for the Rössler systems and resistance $R$ for the electronic circuits. Local linear predictors in the four-dimensional embedding space were built using a learning set of 10 000 pairs $\{d(n),r(n)\}$, and a time delay $T = 5$ in both cases. Transition to a synchronized state is associated with a sharp decrease of $Q$.

chronized state at the same values of coupling; $g \approx 0.18$ for Rössler systems and $R \approx 0.30$ kΩ for electronic circuits.

## VI. CONCLUSION

When one couples two chaotic systems, the natural expectation is that the whole system will perform oscillations, perhaps themselves chaotic, in the full phase space of the two systems. If the two systems are coupled in such a fashion that their variables act synchronously, then clearly only a submanifold of the full joint phase space is being occupied, and this synchronization represents a collapse of evolution in a larger phase space down to this submanifold. We see this in the emergence, for example, of a limit cycle in any individual chaotic system, for the behavior in a phase space of dimension three or larger collapses at some parameter settings to motion on a one-dimensional submanifold: the limit cycle itself. In the case of two coupled chaotic oscillators, the collapse onto the submanifold need not be accompanied by the variables from one oscillator acting in an identical fashion to the variables from the second oscillator. This has been a comfortable and often realized version of the signature of synchronization of coupled systems, but it rests on having both identical systems coupled together and on viewing these identical systems in precisely the same coordinate system. A change of coordinate system by a smooth change of variables, sampling the system through one or a few variables and building up the phase space through time delay embedding, or coupling two nonidentical systems will almost surely result in synchronization that does not manifest itself in the identical temporal evolution of variables from each of the coupled systems.

In this paper we began the exploration, using both simulated and experimental data from nonlinear electrical circuits, of a form of generalized synchronization in which dynamical variables $\mathbf{r}(t)$ from one system, called the response, were determined in terms of the dynamics $\mathbf{d}(t)$ of another, called the drive. We studied here methods for exposing the existence of relationships of the form $\mathbf{r}(t)=\boldsymbol{\psi}(\mathbf{d}(t))$, which collapse the evolution of the full dynamics in $\mathbf{r}(t),\mathbf{d}(t)$ to a submanifold. Collapse of this form we call generalized synchronization as it enlarges our considerations from the most explored case when $\boldsymbol{\psi}(\cdot)$ is the identity. We provided a statistical test called *mutual false nearest neighbors,* which rests on the geometrical idea that when $\mathbf{r}(t)=\boldsymbol{\psi}(\mathbf{d}(t))$ then neighbors in $\mathbf{r}(t)$ space are naturally connected with neighbors in $\mathbf{d}(t)$ space. We were able to show in several examples that this test clearly distinguishes synchronized from nonsynchronized motions in the full $\mathbf{d}(t)\oplus\mathbf{r}(t)$ evolution even when we did not know the function $\boldsymbol{\psi}(\cdot)$ and, indeed, when we only observed one component of the drive or response dynamics and then built the phase spaces by time delay reconstruction.

We also demonstrated, under the same circumstances of ignorance of the synchronization function or of the full dynamical phase space, that the existence of the functional connection $\mathbf{r}(t)=\boldsymbol{\psi}(\mathbf{d}(t))$ implies that the response dynamics is *predictable* in terms of the drive dynamics alone. This is the essence of synchronization in our view, and certainly underlies any applications one would wish to make of the synchronization phenomenon. Our method for establishing this predictability rested on making local polynomial models connecting a variable $r(t)$ from the response system to the drive dynamics as $r(t)=G(\mathbf{d}(t))$. These models were "learned" from joint observations of the response and drive variables and then shown to hold for further observations of the coupled systems. When the systems are synchronized, the errors in learning $G(\cdot)$ are consistently small, and as one changes parameters to desynchronize the coupled oscillators, these errors rise substantially.

In this paper we focused our attention on drive and response systems, which were coupled unidirectionally. No feedback from the response system back to the drive was considered. Clearly this is only a subset of the possible settings where synchronization can occur. Our geometric and predictability tests for synchronization will be valid and useful in the much larger class of possible couplings and mutual feedbacks, which may occur among dynamical oscillators. Our choice of unidirectional coupling was made to allow us to establish clearly synchronized systems, which we could then examine in changed coordinate systems and which we could then analyze using time delay embedding, and do all this in circumstances where we knew the parameter regimes where synchronization occurs and regimes where it does not.

The methods developed here will have wide applicability to other situations where we do not know beforehand the kind of behavior—synchronized or unsynchronized—and we shall utilize our tools for the analysis of such systems in our work to follow this article.

## ACKNOWLEDGMENTS

We are very grateful to our colleagues at the Institute for Nonlinear Science for fruitful discussions. The contributions of M. Kennel, R. Brown, and M. Rabinovich were especially helpful. This work was supported in part by the U.S. Department of Energy, Office of Basic Energy Sciences, Division of Engineering and Geosciences, under Contract No. DE-FG03-90ER14138, and in part by the Army Research Office (Contract No. DAAL03-91-C-052), and by the Office of Naval Research (Contract No. N00014-91-C-0125), under subcontract to the Lockheed/Sanders Corporation.

## APPENDIX

In the main body of the paper we discussed several examples of pairs of coupled systems that exhibit generalized synchronization of chaos. These pairs were produced by applying a transformation to identical systems that had synchronized in the sense that the dynamical variables in the driving system and in the response system demonstrated identical oscillations. Here we give a general context to those changes of variable that illustrate the details of this procedure.

### 1. Response systems transformed by an algebraic relation

A particularly simple case occurs when we change response variables using a local algebraic vector function. Suppose we change the variables in (4) from $\mathbf{y}$ to

$$\mathbf{z}=\boldsymbol{\phi}(\mathbf{y}) , \tag{A1}$$

where $\boldsymbol{\phi}$ is a continuous invertible vector function. Differentiating (A1) with respect to time and using (4), the evolution of the $\mathbf{z}(t)$ is

$$\frac{d\mathbf{z}}{dt}=\mathbf{J}\cdot\mathbf{F}(\boldsymbol{\phi}^{-1}(\mathbf{z}))-\mathbf{J}\cdot\mathbf{G}\cdot[\boldsymbol{\phi}^{-1}(\mathbf{z})-\mathbf{x}(t)] , \tag{A2}$$

where

$$\mathbf{J}=\left.\frac{\partial\boldsymbol{\phi}}{\partial\mathbf{r}}\right|_{\mathbf{r}=\boldsymbol{\phi}^{-1}(\mathbf{z})} . \tag{A3}$$

If the coupled driving and response systems exhibited simple synchronization with $\mathbf{y}(t)=\mathbf{x}(t)$, then the relationship in $(\mathbf{z}(t),\mathbf{x}(t))$ space will not be so clean. Nonetheless, we would agree that the driver and the response are synchronized even though we were not so fortunate as to choose the "best" coordinates. This is more than just a semantic issue arising from a self-imposed change of coordinates since, in dealing with observed data, the coordinates we end up working with are the time delays of the observed dynamical variables, and these may not be best—except that we have no other.

### 2. Integral-algebraic variable changes

The method that we used to produce system (22) can be given in a general form. To do so we start with driving and response systems (3) and (4) which, under appropriate choice of $\mathbf{G}$ exhibit identical chaotic motions (5). To introduce the effects of short-term memory into the system, we supplement the driving and response systems with dynamical variables $\mathbf{x}_m$ and $\mathbf{y}_m$, correspondingly, which evolve according to

$$\begin{aligned}\frac{d\mathbf{x}_m(t)}{dt}&=\mathbf{H}(\mathbf{x}_m(t),\mathbf{x}(t)) ,\\ \frac{d\mathbf{y}_m(t)}{dt}&=\mathbf{H}(\mathbf{y}_m(t),\mathbf{y}(t)) ,\end{aligned} \tag{A4}$$

to form the augmented driving system

$$\frac{d\tilde{\mathbf{x}}(t)}{dt}=\mathbf{Q}(\tilde{\mathbf{x}}(t))\equiv\begin{cases}\dfrac{d\mathbf{x}(t)}{dt}=\mathbf{F}(\mathbf{x}(t))\\ \dfrac{d\mathbf{x}_m(t)}{dt}=\mathbf{H}(\mathbf{x}_m(t),\mathbf{x}(t))\end{cases} \tag{A5}$$

and the augmented response system for variable $\tilde{\mathbf{y}}$

$$\begin{aligned}\frac{d\tilde{\mathbf{y}}(t)}{dt}&=\mathbf{Q}(\tilde{\mathbf{y}}(t))-\boldsymbol{\Gamma}(\tilde{\mathbf{y}}(t)-\tilde{\mathbf{x}}(t))\\ &\equiv\begin{cases}\dfrac{d\mathbf{y}(t)}{dt}=\mathbf{F}(\mathbf{y}(t))-\mathbf{G}(\mathbf{y}(t)-\mathbf{x}(t))\\ \dfrac{d\mathbf{y}_m(t)}{dt}=\mathbf{H}(\mathbf{y}_m(t),\mathbf{y}(t)) ,\end{cases}\end{aligned} \tag{A6}$$

where $\boldsymbol{\Gamma}$ has the form

$$\begin{bmatrix}\mathbf{G} & 0\\ 0 & 0\end{bmatrix} . \tag{A7}$$

There are some limitations imposed on the choice of systems which describe time evolution of the vectors of the variables $\mathbf{x}_m(t)$ and $\mathbf{y}_m(t)$. These limitations come from the condition that this system does not introduce new active degrees of freedom. To satisfy this, the dynamics of $\mathbf{x}_m(t)$ can be selected so there is an attractor in $\tilde{\mathbf{x}}$ space, and as $t\to\infty$, $\mathbf{x}_m(t)$ becomes independent of its initial value $\mathbf{x}_m(0)$. In this case, the behavior of system (A5) is completely determined by the dynamics generated by $\mathbf{F}(\mathbf{x})$. The role of the $\mathbf{x}_m(t)$ variables is to provide a simple filtering of the $\mathbf{x}(t)$ dynamics of the driving system and to introduce time delays in the response of $\tilde{\mathbf{x}}(t)$ alone. A similar situation occurs in the problem of synchroniza-iton and communications using filtered signals [29].

Now we consider a new response system $\tilde{\mathbf{z}}$ produced by a change of variables

$$\tilde{\mathbf{z}}=\boldsymbol{\chi}(\tilde{\mathbf{y}}) . \tag{A8}$$

The new response system $\tilde{\mathbf{z}}$ is given by

$$\frac{d\tilde{\mathbf{z}}}{dt}=\mathbf{J}\cdot\mathbf{Q}(\boldsymbol{\chi}^{-1}(\tilde{\mathbf{z}}))-\mathbf{J}\cdot\boldsymbol{\Gamma}\cdot(\boldsymbol{\chi}^{-1}(\tilde{\mathbf{z}})-\tilde{\mathbf{x}}(t)) , \tag{A9}$$

where

$$\mathbf{J}=\left.\frac{\partial\boldsymbol{\chi}}{\partial\tilde{\mathbf{y}}}\right|_{\tilde{\mathbf{y}}=\boldsymbol{\chi}^{-1}(\tilde{\mathbf{z}})} . \tag{A10}$$

As was pointed out in the preceding section, the system (A6) can be synchronized by driving $\tilde{\mathbf{x}}$ and, therefore, the system $\tilde{\mathbf{z}}$ can also be synchronized by the same driving. The equation governing the evolution of $\mathbf{x}_m(t)$ decouples from the rest of equations in systems (A5) and (A9). Thus, we constructed a response system $\tilde{\mathbf{z}}$, whose space of actual variables has a dimension higher than that of the phase space of the driving system $\tilde{\mathbf{x}}$, but which still can be synchronized by system $\tilde{\mathbf{x}}$.

When systems (A5) and (A6) [or, equivalently, systems (A5) and (A9)] are synchronized $\mathbf{y}_m(t)=\mathbf{x}_m(t)$. On the other hand, the fact that the equations for $\tilde{\mathbf{x}}_m$ decouple from the rest of equations and the restrictions that we applied on the choice of $\mathbf{x}_m$ imply that $\mathbf{x}_m$ can be obtained from $\mathbf{x}$ by means of some integral transformation $\boldsymbol{\Upsilon}$ which is, in general, nonlinear. Thus, when the systems are synchronized we have $\mathbf{y}_m(t)\equiv\mathbf{x}_m(t)=\boldsymbol{\Upsilon}(\mathbf{x}(t))$ and, naturally, $\tilde{\mathbf{y}}(t)=\tilde{\mathbf{x}}(t)$. Therefore, relation (A8) means that systems (3) and (A9) are synchronized in the sense that $\tilde{\mathbf{z}}(t)=\boldsymbol{\Theta}(\mathbf{x}(t))$ where $\boldsymbol{\Theta}$ is some integral transformation which is, in general, nonlinear. Relation (23), which was derived above for synchronization of Rössler-like systems, is an example of the transformation $\boldsymbol{\Theta}$.

[1] H. Fujisaka and T. Yamada, Prog. Theor. Phys. **69**, 32 (1983).
[2] V. S. Afraimovich, N. N. Verichev, and M. I. Rabinovich, Radiophys. Quantum Electron. **29**, 795 (1986).
[3] L. M. Pecora and T. L. Carroll, Phys. Rev. Lett. **64**, 821 (1990).
[4] T. L. Carroll, and L. M. Pecora, Physica D, **67**, 126 (1993).
[5] A. R. Volkovskii and N. F. Rulkov, Pis'ma Zh. Tekh. Fiz. **19**, 71 (1993) [Tech. Phys. Lett. **19**, 97 (1993)].
[6] K. S. Halle, Ch. W. Wu, M. Itoh, and L. O. Chua, Int. J. Bifurc. Chaos Appl. Sci. Eng. **3**, 469 (1993).
[7] K. Pyragas, Phys. Lett. A **170**, 421 (1992).
[8] N. F. Rulkov, L. S. Tsimring, and H. D. I. Abarbanel, Phys. Rev. E. **50**, 314 (1994).
[9] A. V. Gaponov-Grekhov, M. I. Rabinovich, and I. M. Starobinets, Pis'ma Zh. Eksp. Teor. Fiz. **39**, 545 (1984) [JETP Lett. **39**, 667 (1984)].
[10] H. G. Winful and Lutfur Rahman, Phys. Rev. Lett. **65**, 1575 (1990).
[11] T. L. Carroll and L. M. Pecora, IEEE Trans. Circuits Syst. **38**, 453 (1991).
[12] N. F. Rulkov, A. R. Volkovskii, A. Rodriguez-Lozano, E. Del Rio, and M. G. Velarde, Int. J. Bifurc. Chaos **2**, 669 (1992).
[13] N. F. Rulkov and A. R. Volkovskii, in *Choas in Communications,* edited by Louis M. Pecora, SPIE Proc. Vol. 2038 (SPIE, Bellingham, WA, 1993) p. 132.
[14] M. Ding and E. Ott, Phys. Rev. E **49**, R945 (1994).
[15] T. C. Newell, P. M. Alsing, A. Gavrielides, and V. Kovanis, Phys. Rev. E **49**, 313 (1994).
[16] T. C. Newell, P. M. Alsing, A. Gavrielides, and V. Kovanis, Phys. Rev. Lett. **72**, 1647 (1994).
[17] A. R. Volkovskii and N. F. Rulkov, Pis'ma Zh. Tekh. Fiz. **15**, 5 (1989) [Sov. Tech. Phys. Lett. **15**, 249 (1989)].
[18] V. S. Anischenko, T. E. Vadivasova, D. E. Postnov, and M. A. Safanova, Int. J. Bifurc. Chaos **2**, 633 (1992).
[19] R. Mañe, in *Dynamical Systems and Turbulence, Warwick 1980,* edited by D. Rand and L. S. Young, Lecture Notes in Mathematics Vol. 898 (Springer, Berlin, 1981).
[20] F. Takens, in *Dynamical Systems and Turbulence, Warwick 1980* (Ref. [19]).
[21] H. D. I. Abarbanel, R. Brown, J. J. Sidorovich, and L.SS.Tsimring, Rev. Mod. Phys. **65**, 1331 (1994).
[22] H. D. I. Abarbanel, T. A. Carroll, L. M. Pecora, J. J. Sidorovich, and L. S. Tsimring, Phys. Rev. E **49**, 1840 (1994).
[23] R. Brown, N. F. Rulkov, and E. R. Tracy, Phys. Rev. E **49**, 3784 (1994).
[24] A. R. Volkovskii and N. F. Rulkov, Pis'ma Zh. Tekh. Fiz. **14**, 1508 (1988) [Sov. Tech. Phys. Lett. **14**, 656 (1988)].
[25] M. B. Kennel, R. Brown, and H. D. I. Abarbanel. Phys. Rev. A **45**, 3403 (1992).
[26] N. Platt, E. A. Spiegel, and C. Tresser, Phys. Rev. Lett. **70**, 279 (1993).
[27] E. Ott and J. C. Sommerer, Phys. Lett. A **188**, 39 (1994).
[28] N. F. Rulkov, A. R. Volkovskii, A. Rodriguez-Lozano, E. Del Rio, and M. G. Velarde, Chaos Solitons Fractals **4**, 201 (1994).
[29] T. L. Carroll, Phys. Rev. E **50**, 2580 (1994).